Icarus 206 (2010) 382–389

Contents lists available at ScienceDirect

Icarus

journal homepage: www.elsevier.com/locate/icarus

The structure and time variability of the ring atmosphere and ionosphere

W.-L. Tseng [a,*], W.-H. Ip [a], R.E. Johnson [b], T.A. Cassidy [b], M.K. Elrod [b]

[a] Institute of Astronomy, National Central University, No. 300, Jhongda Rd., Jhongli 320, Taiwan
[b] Department of Materials Science & Engineering, University of Virginia, Charlottesville, VA 22903, USA

ARTICLE INFO

Article history:
Received 5 February 2009
Revised 20 May 2009
Accepted 25 May 2009
Available online 6 June 2009

Keywords:
Saturn
Rings
Atmosphere
Magnetosphere

ABSTRACT

The saturnian system is subject to constant bombardment by interplanetary meteoroids and irradiation by solar UV photons. Both effects release neutral molecules from the icy ring particles either in the form of impact water vapor or gas emission in the form of H_2O, O_2 and H_2. The observations of the Cassini spacecraft during its orbit insertion have shown the existence of molecular and atomic oxygen ions. Subsequent modeling efforts have led to the picture that an exospheric population of neutral oxygen molecules is probably maintained in the vicinity of the rings via photolytic-decomposition of ice and surface reactions. At the same time, ionized products O^+ and O_2^+ ions move along the magnetic field lines and, depending on the optical local thickness rings, can thread through the ring plane or impact a ring particle, the ion principal sink. In addition, collisional interactions between the ions and neutrals will change the scale height of the ions and produce a scattered component of O_2 molecules and O atoms which can be injected into Saturn's upper atmosphere or the inner magnetosphere. The ring atmosphere, therefore, serves as a source of O_2^+ ions throughout Saturn's magnetosphere. If photolysis of ice is the dominant source of O_2, then the complex structure of the ring atmosphere/ionosphere and the injection rate of neutral O_2 will be subject to modulation by the seasonal variation of Saturn along its orbit. In this work, we show how the physical properties of the ring oxygen atmosphere, the scattered component, and the magnetospheric O_2^+ ion source rate vary as the ring system goes through the cycle of solar insolation. In particular, it is shown that the magnetopheric O_2^+ ions should be nearly depleted at Saturn's equinox if O_2 is produced mainly by photolysis of the ring material.

© 2009 Elsevier Inc. All rights reserved.

1. Introduction

Because of its icy water composition, the saturnian ring system has been suggested to be a source of a neutral atmosphere due to photosputtering (e.g., Carlson, 1980) and the bombardment of interplanetary meteoroids (Ip, 1984a). The photosputtering rate is $\sim 10^9$ $H_2O/cm^2/s$ (Westley et al., 1995) and the impact vapor production rate is 5×10^{27} H_2O s^{-1} using a meteoroid mass impact flux $\sim 6 \times 10^4$ g s^{-1} (Ip, 1984a), although much larger impact rates have been suggested (e.g., Morfill et al., 1983). Although H_2O, OH and O are the principal products, molecular oxygen was seen to be a principal component of the ring ionosphere (Tokar et al., 2005) suggesting that oxygen molecules dominate the tenuous ring atmosphere (Johnson et al., 2006). This is the case because O_2 can form via surface chemical reactions of the water-dissociated products like O and OH (Ip, 1995) and O_2, along with H_2, can be directly emitted from the ring particle surfaces via photolytic-decomposition of ice (e.g., Johnson and Quickenden, 1997). Since H_2O molecules tend to recondense on the ring particles during re-impact and H_2 escapes more readily from the ring system (Johnson et al., 2006), O_2 is the main composition of the ring atmosphere. It has also been shown that the ions and charged grains created in the vicinity of the ring plane are subject to both the gravitational force of Saturn and electromagnetic force possibly leading to large-scale mass transport effect (Connerney et al., 1983; Ip, 1984a,b). In this paper we re-examine the morphology of and particles dynamics occurring in Saturn's ring atmosphere and ionosphere, as well as the rate at which this atmosphere supplies oxygen to the thermosphere of Saturn and molecular oxygen ions to Saturn's magnetosphere beyond the outer edge of the main rings.

When Cassini spacecraft flew over Saturn's main ring system on 1 July 2004, both the Cassini Plasma Instrument (CAPS) and the Ion Neutral Mass Spectrometer (INMS) detected O^+ and O_2^+ ions above the main rings (Young et al., 2005; Tokar et al., 2005; Waite et al., 2005) as well as a comparable component of electrons (Coates et al., 2005). These detections confirmed the existence of the ring atmosphere and ionosphere providing the first definitive number densities for the spatial distribution and composition of the plasma. Using these ion densities, initial assessments of the neutral densities were made by Ip (2005) and Johnson et al. (2006). In addition, from Cassini RPWS measurements, Farrell et al. (2008) found locations where plasma mass from the ring-ionosphere is

* Corresponding author.
E-mail address: d939006@astro.ncu.edu.tw (W.-L. Tseng).

0019-1035/$ - see front matter © 2009 Elsevier Inc. All rights reserved.
doi:10.1016/j.icarus.2009.05.019

possibly loaded at 1–2 kg s^{-1} onto field lines near the Cassini Division. Since molecular oxygen from the ring atmosphere is scattered into the magnetosphere (Johnson et al., 2006), Martens et al. (2008) suggested that the O_2^+ detected by CAPS, with a density ratio $\sim 0.003 O_2^+/H_2O$ for $L = 4.5$–8, may have originated from the ring atmosphere.

This wealth of data has led to important revisions in our picture of the ring atmosphere. For example, in the absence of ion–molecule collisions, the neutral O_2 would be confined to the ring region with a very small scale height (~1000 km) determined by the local ring temperature. Therefore, the photoionized products of O_2, such as O_2^+ and O^+, would form near the ring plane with velocities similar to the local Keplerian velocities plus small thermal velocities. These ions would have pitch angles near 90° and low mirror altitudes. But such a spatial distribution could not account for the Cassini observations of a significant ion density well above the ring plane. Johnson et al. (2006) suggested that the ion–molecule collisions between the newly formed ions O_2^+ and O^+ and neutral O_2 could have important effects. First, the scattered O_2^+ and O^+ ions can attain velocity distributions with much larger mirror altitudes, consistent with the Cassini detections. Second, the scattered O_2 could also impact into Saturn's atmosphere and be injected into the magnetosphere. Luhmann et al. (2006) modeled the ring ionosphere taking into consideration of the offset of the dipole field and of the charge-exchange scattering of ions. They showed that an asymmetry above and below the ring plane should exist in the inner ring ionosphere. As a result, ions precipitate into Saturn's atmosphere mainly on the southern hemisphere due to the northward offset in the dipole filed. Subsequently, Bouhram et al. (2006) used a test particle model with a Monte-Carlo method to simulate the ring atmosphere/ionosphere system confirming the general spatial variation in the densities of O_2^+ and O^+ and the enhancements in the Cassini gap seen by CAPS.

Previous works of Luhmann et al. (2006) and Bouhram et al. (2006) have focus on the ions in the main ring, and Johnson et al. (2006) used a simple analytic model to describe the distribution of neutral O_2. A model of the co-existence of the ring atmosphere and ionosphere requires a self-consistent treatment of the dynamical coupling of the ions and neutrals. Therefore, in order to describe the spatial distributions and transport of the ring ions and neutrals, especially those produced by ion-molecule interactions, we have developed a Monte-Carlo method to simulate the test particle motion of both the neutrals and ions. As in Bouhram et al. (2006), Saturn's gravity, the corotation electric field and the dipole field with northward offset to $0.04R_S$ (Connerney et al., 1983) are all taken into account in the computation of ion trajectories. In addition, chemical processes, such as photolytic reactions and ion-neutral reactions, are considered. Details of these simulations are given in Section 2. In Section 3, we give the results specific to the Saturn Orbit Insertion (SOI) trajectory when the Sun was below the ring plane with a solar insolation angle of 24°. The main features of this new steady state model will be compared to previous simulation results. Because of the importance of oxygen in Saturn's thermosphere, we estimate the injection rate of oxygen from the ring atmosphere into Saturn's upper atmosphere by ion–molecule collisions. In order to help describe the composition of Saturn's magentospheric plasma, we also determine the injection rate of the neutral O_2 molecules of ring origin into the inner magnetosphere which could be a significant source of both the O_2^+ ions detected by CAPS in the inner magnetosphere as well as a source of the energetic O_2^+ ions detected by the MIMI instrument (Krimigis et al., 2005). These estimates will be reported in Section 3. As Saturn orbits around the Sun, the solar insolation angle varies between 0° (i.e. edge-on illumination of the rings) and 25° above and below the ring plane. Therefore, the physical conditions of the ring atmosphere and ionosphere should exhibit seasonal variations. This is only true if photolytic decomposition of ice is the main source of the O_2 molecules. The possible seasonal-variations will be discussed in Section 4. A discussion will be given in Section 5 to be followed by a summary in Section 6.

2. Model descriptions

2.1. A model of the O_2 atmosphere

We first simulate the situation with the Sun at 23.6 degrees south of the ring plane when Cassini flew above the ring plane on 1 July 2004. It is assumed that O_2 production is dominated by the decomposition of ice by radiolysis as proposed in Johnson et al. (2006). This would imply that H_2 is also ejected in a two to one ratio. Here we examine the distributions of both oxygen ions and neutrals. This is done in an iterative manner as outlined in the flow chart in Fig. 1.

The UV photons are subject to the absorption effect of the ring particles, and the flux on the sunlit side is modified by a factor of $(1-f)$ and $f = \exp(-\tau/\cos\gamma)$ which is determined by the optical thickness of the ring τ and $\gamma = 66.4°$ is the incident angle of UV photons to the ring plane normal. For simplicity, we set the optical thickness τ to be 0.5, 1.0 and 0.01 for the A, B and C ring, respectively (Esposito et al., 1983). The neutral O_2 production rate is then given as $Q(O_2)*(1-f)*A*\cos\gamma$ where A is the area of the rings. In this work, we use $Q(O_2) = 10^6$ molecules cm^{-2} s^{-1} (Johnson et al., 2006). In this simulation O_2 is injected in a random direction from the ring plane with an initial weighting factor according to the ring optical thickness. From our numerical calculations, it is found that the columns of O_2 above and below the ring plane are nearly the same because the O_2 has a long lifetime and interacts frequently with the ring particles during its multiple orbits (Johnson et al., 2006). The initial ejection velocity of O_2 test particle is the local Keplerian velocity of the ring particle plus an ejection velocity in a random direction with a non-thermal energy distribution described by $F(E) \sim U/(E+U)^2$ where $U = 0.015$ eV (Johnson et al., 1983).

As shown in Fig. 1, the ejected O_2 is tracked in its orbit until it is either destroyed photolytically, scattered by an ion or, most often, returns to the ring plane and impacts a ring particle. The O_2 molecules moving across the ring plane can be absorbed by a ring particle with the probability of $P = 1 - \exp(-\tau/\cos\alpha)$, where τ is the optical depth at the point of impact and α is the incident angle between the O_2 velocity in the rotating frame of the ring and the normal to the ring plane. In the A and B ring regions, the absorption probability is high ($P > 0.5$). Unlike H_2O, the O_2 molecules do not permanently stick on the icy ring particles at the expected low temperature (~100 K). Therefore, the temporarily absorbed O_2 will accommodate to the ring particle temperature and be subsequently ejected with a Maxwellian distribution of velocities determined by the local surface temperature of the ring particles. The ejected O_2 test particle is again tracked until it is destroyed, scattered or re-impacts a ring particle.

In order to account for photolytic loss, the weighting factor of each test particles is reduced by a value of $\exp(-\Delta t/T_{Loss})$ in an integration time step (Δt) where T_{Loss} is the photolytic destruction time scale. Direct loss of neutral O_2 by scattering into Saturn's atmosphere or injection into orbital motion outside a radial distance of $20R_S$ is also accounted for.

We also model the structure of the oxygen atomic component of the ring atmosphere. Neutral O is produced from the photodissociation of O_2 at a rate $K = 5.88 \times 10^{-8}$ s^{-1} (Huebner et al., 1992). The main difference between O_2 and O is that each O fragment is formed with the velocity of the parent O_2 plus a large excess energy ~0.8 eV in random direction (e.g., Johnson et al., 2006).

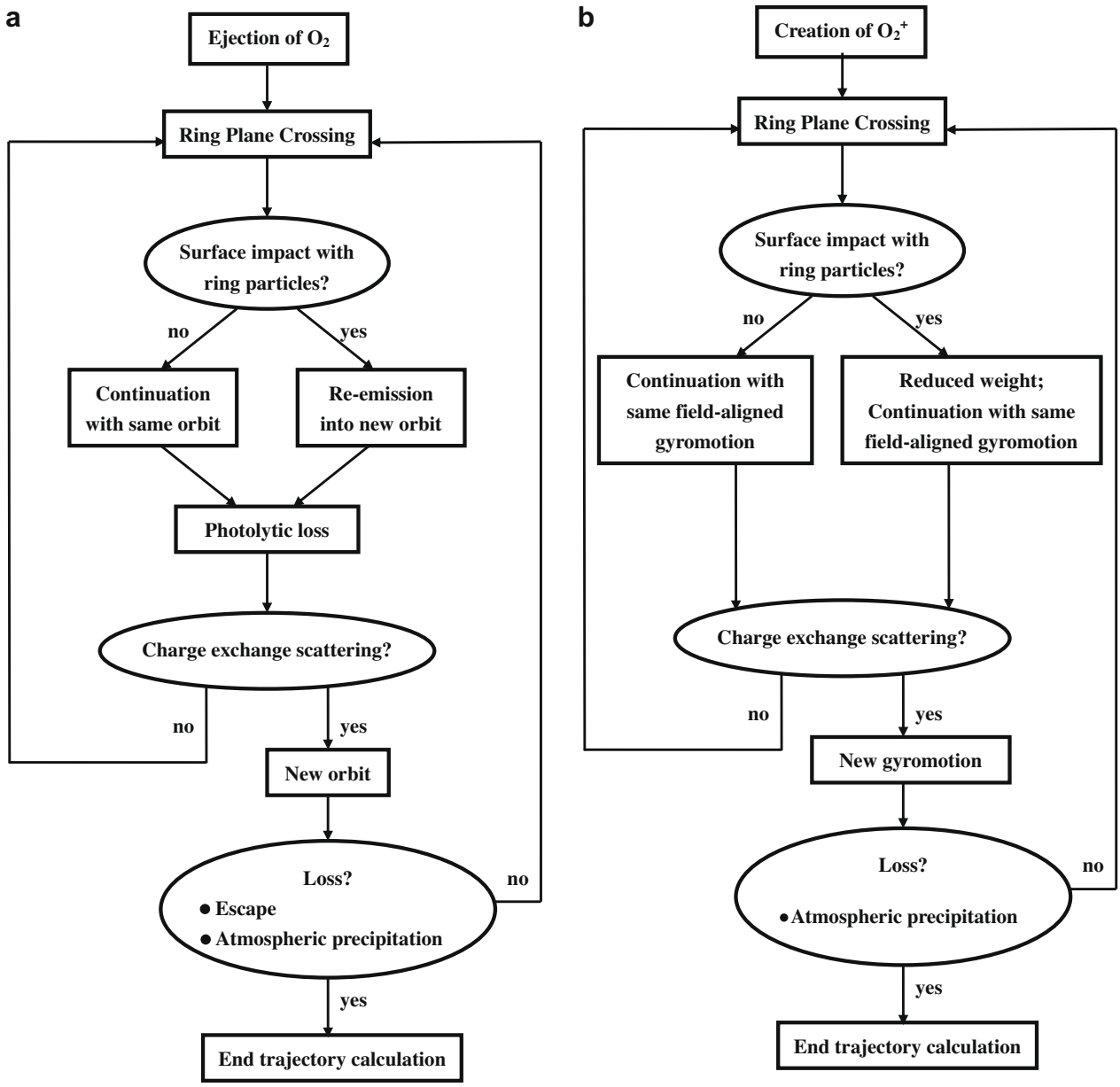

Fig. 1. (a) The flow chart of the Monte-Carlo procedure on the trajectory calculation of neutral O_2. (b) The flow chart of the Monte-Carlo procedure on the trajectory calculation of O_2^+ ions.

Therefore, the O component of the atmosphere has a much larger scale height than that of the O_2 component.

The neutral production is simulated by injection of 20,000 O_2 test particles randomly from the main ring regions between 1.24 and 2.4R_S. The source strength vs different radial distance is represented by assigning weighting factors with initial values determined by the local optical depth. Their subsequent Keplerian motion is calculated using a Runge–Kutta integration routine with a fixed time steps ($\Delta t = 0.8$ s). The ions are assumed to be produced predominantly by photoionization of the neutral ring atmosphere. Immediately after production, the new ions will be subject to the electromagnetic force as described below. The trajectory calculations of the neutrals are stopped when they are lost to the planetary atmosphere or when they move outside a radial distance of 20R_S. The numerical computation of a test particle will also stop if the corresponding weighting factor is less than 0.01. By the same token, ions are lost via ring absorption according to the local optical depth or by precipitation into Saturn's atmosphere as discussed further below. As discussed before, the ring neutrals and ions are coupled via relatively low energy ion-neutral collisions which turn out to play an important role in redistributing their orbital motions (Johnson et al., 2006). In calculating the source rates and the neutral and ion densities, the 3D-grid system is divided into $120 \times 200 \times 160$ grid points with $\Delta\theta = 3°$, $\Delta R = 0.05R_S$ and $\Delta Z = 0.02R_S$. As mentioned above, the computations are done iteratively until equilibrium is reached as described in the flow chart of our computation in Fig. 1a and b. In our modeling, the real number density is obtained by scaling the simulated number density by a conversion factor of the total number of test particle employed to the photoproduction rate, which was proposed by Ip (1995).

Note that most of the O atoms and the atomic and molecular oxygen ions are absorbed by impact on the ring particles. Since these are reactive they can induce chemistry on the surface of the ice grains and be recycled into O_2. In order to account for

recycling of O_2 into the ring atmosphere, we can use a factor C_r, which is the fraction of returned ions and O atoms which are absorbed by the ring particles. Since we do not track O^+ we use C_r are 0.4 and 0.85 for O_2^+ ions and O atoms, respectively. The would be to increase the oxygen number density by a factor of 4.5 ($f_i + f_o$), with $f = 1 + C_r/(1 - C_r)$ for the ion and the neutral. Because recycling as O would be limited by the return of hydrogen, Johnson et al. (2006) estimated the ratio of the loss rate for two hydrogen to the loss rate for one oxygen to be >∼10. These estimates would imply that the steady state O_2 and O_2^+ column densities and O_2^+ scattering rate in our results could be probably multiplied by a factor of about 5–10.

2.2. Ion production and transport

O_2^+ and O^+ are formed from photoionization and photodissociation of O_2 at a rate $K_i = 9.1 \times 10^{-9}\ s^{-1}$ and $K_d = 2.5 \times 10^{-9}\ s^{-1}$, respectively. Because of the ring shadow effect, ionization rates in the sunlit and sunshade sides of the ring plane differ as determined by the local optical thickness. That is, the ionization rates in the shadow zone will be reduced by a factor of $\exp(-\tau/\cos\gamma)$. At production and prior to pick-up acceleration, the new O_2^+ ions will have the same velocity of the O_2 molecules which is small. However, the O^+ ions will have an additional random velocity due to the excess energy of about 0.5 eV from the photodissociation process of $O_2 + h\upsilon \rightarrow O + O^+ + \Delta\varepsilon$ (e.g., Johnson et al., 2006). When ions form in the vicinity of the ring plane, they are picked up by Saturn's magnetic field in a time fast compared to the integration time step. The local corotational electric field at pick-up is $\mathbf{E} = -\mathbf{V_{CO}} \times \mathbf{B}$ where $\mathbf{V_{CO}}$ is the corotational velocity and B is the local magnetic field. This is treated as a dipole field with a northward shift of $0.04R_S$ (Connerney et al., 1983). The equation of motion of the ions is determined by the gravitational force and the Lorentz force,

$$\mathbf{m}d\mathbf{V}/d\mathbf{t} = -\mathbf{GM}/\mathbf{r^2} + \mathbf{q}(\mathbf{E} + \mathbf{V} \times \mathbf{B}) \quad (1)$$

where $\mathbf{V}$ is the ion velocity, is solved by using the Runge–Kutta method. A new O_2^+ ion is formed initially with the local Keplerian velocity plus the thermal velocity in random direction. On pick-up the ions are accelerated by the corotational electric field so that, in the absence of Saturn's gravity they gyrate about the magnetic field at a speed $\sim V_K - V_{CO}$ and orbit the planet at V_{CO}. However, as the distance from Saturn decreases the relative importance of the Lorentz and planetary gravitational forces changes affecting the subsequent motion along the local magnetic field line. If Saturn's gravity is ignored these ions that are not formed at the magnetic equator should move along the field lines and oscillate about the magnetic equator. As will be described in more detail later, Saturn's gravitational force tends to pull the ions down from the magnetic equator towards the planet. In Fig. 2, it is shown that O_2^+ ions created close to the ring plane and within a radial distance, $R_C \sim 1.7R_S$, inside of which $V_K < V_{CO}$, precipitate with near unit efficiency into Saturn's southern atmosphere (Connerney et al., 1983; Ip, 1984c; Luhmann et al., 2006). Ions created outside R_C can mirror and be lost to by ring collision with ring particles before precipitating into Saturn's atmosphere as described earlier (Luhmann et al., 2006; Bouhram et al., 2006).

In tracking the O_2^+ ions we have ignored electron-recombination producing two energetic O atoms, since the computed electron densities are very low. This is also consistent with the Cassini measurements above the ring plane at SOI (Young et al., 2005; Krimigis et al., 2005; Coates et al., 2005). In addition, we have also ignored neutralization of the ions on the surface of the grains which would directly recycle them as neutrals into the ring atmosphere.

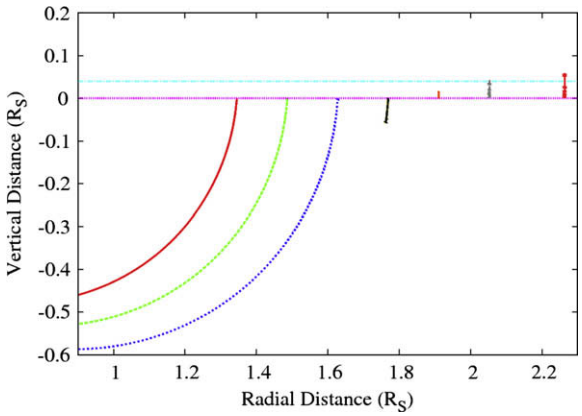

Fig. 2. The trajectories of the O_2^+ ion motion in different radial distances from Saturn. The ions are created with the local Keplerian velocity on the ring plane ($Z = 0$). (Black dash horizontal line: the ring plane; orange dash-dotted horizontal line: the magnetic equator.)

2.3. Ion–molecule charge exchange reactions

In describing motion of the ions about the magnetic equator, their interaction with the neutrals is treated iteratively. In addition, since the ion-neutral collisions speeds are low (energies ≪ eV/amu), ion–molecule reactions are important. The scattering cross-sections for $O_2^+ + O_2 \rightarrow O_2^+ + O_2$ and $O_2^* + O_2^+$ have values roughly determined by the Langevin rate constant 7.4×10^{-10} $cm^{-3}\ s^{-1}$ (Johnson et al., 2006). After a collision, each species has a new velocity in the inertial frame, the initial velocity of the center of mass plus a velocity in a random direction that is equal to half of the relative collision speed. The out-going velocity after the scattering is written in the form of

$$v_x = V_{CM\_X} + (m/M) \times v_{rel} \times \cos(\alpha) \times \sin(\theta) \quad (2)$$

$$v_y = V_{CM\_Y} + (m/M) \times v_{rel} \times \sin(\alpha) \times \sin(\theta) \quad (3)$$

$$v_z = V_{CM\_Z} + (m/M) \times v_{rel} \times \cos(\theta) \quad (4)$$

where V_{CM} is the velocity of the center of mass, v_{rel} is the relative velocity between the ion and the neutral, m is the O_2 mass and M (=2m) is the total mass. In the Monte-Carlo calculation, the relative velocity is given randomly (α: azimuthal angle; θ: polar angle). Therefore, neutral O_2 can attain a velocity very different from its initial Keplerian velocity and be scattered into Saturn's upper atmosphere or into the magnetosphere where it can be a source of magnetospheric O_2^+ detected by Cassini (Martens et al., 2008). Due to the low O^+ density we do not take into account the momentum transfer collision $O^+ + O_2 -> O^+ + O_2$ with a rate ($K = 6.17 \times 10^{-10}$ $cm^{-3}\ s^{-1}$; Johnson et al., 2005).

3. Saturn orbit insertion conditions

During the SOI the sunlit side was below the ring plane with the incidence angle of UV photons to the normal of the ring plane about 66°. The spatial distribution of the O_2 molecules assuming steady state condition is shown in Fig. 3. These results are in general agreement with those in Johnson et al. (2006) and Bouhram et al. (2006), but the details differ in a number of ways, as described in the following.

It can be seen in Fig. 3a that the neutral gas is concentrated in a flat disk with a total vertical thickness of about $0.08R_S$ (∼4800 km). The bulk of the atmosphere is confined between the outer edge of the A ring ($2.28R_S$) and extends to the inner edge of the C ring ($1.24R_S$). There are a number of noteworthy features resulting from the ballistic transport of the O_2 molecules across the ring plane which can be best described by examining the radial distribution

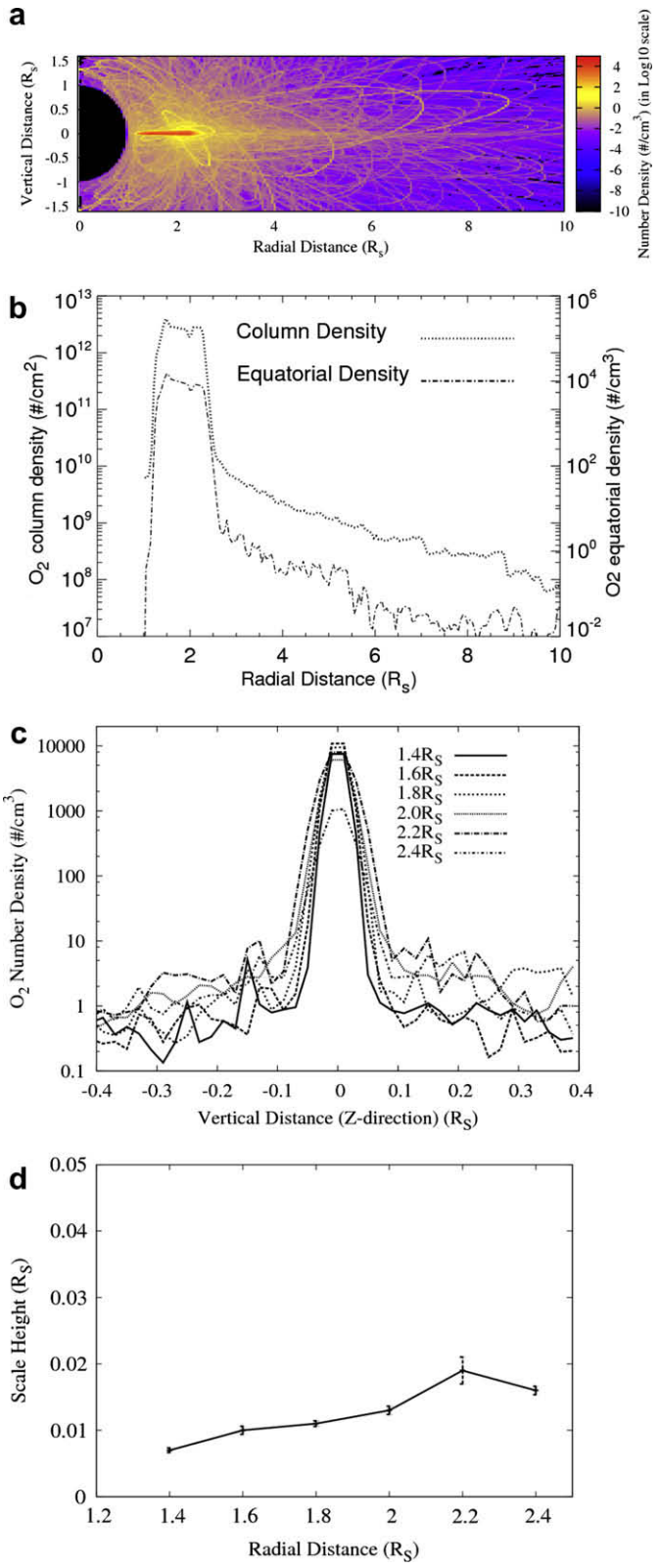

Fig. 3. (a) The neutral O_2 number density. The color is the density (#/cm^3) in Log10 scale. (b) The O_2 column density with variation of radial distance (solid line). The O_2 number density in the equatorial plane (dash-dotted line). (c) The O_2 number density along the Z-direction in the different radial distances. (d) The neutral O_2 scale height in the radial distances in the equatorial plane.

of the column density (solid line) and the number density in the equatorial plane (dash-dotted line) given in Fig. 3b. First, the column density is much smoother than would be predicted by the simple analytical model in Johnson et al. (2006) where the local column is roughly proportional to the local source rate. Note that, there is a depletion of the column density at the Cassini Division. However, due to ballistic transport into this region from the A and B rings, this depletion is much less severe than expected from the decrease in the local source rate. At the boundary between the B and C rings, we find the existence of a density peak. This is caused by the sharp discontinuity at this location which permits the O_2 molecules moving from the B ring to accumulate (Ip, 1983). The radial distribution of neutral O_2 number density in the equatorial plane also follows in this trend. Fig. 3c shows the neutral O_2 equatorial number density corresponding to the vertical distances as a function of radial distance. It is seen that the scale heights increases slightly with increasing radial distance in the main ring region consistent with a decrease in the gravitational confinement (as shown in Fig. 3d).

Even though the column number density falls sharply outside the outer edge of the A ring, an extended distribution exists to beyond $10R_S$. This external population is generated by scattering due collisions between O_2 and O_2^+ as described in the previous section. This scattered contribution agrees with that calculated by Johnson et al. (2006) and shown in Martens et al. (2008). However, here the statistics are considerably improved showing a smooth decay in the column density vs. distance from the outer edge of the A ring. We have an approximate fit to the variation of column density, N_{O2}, outside $3.0R_S$: with increasing radial distances in the equatorial plane, R_p, $N_{O2} = N_{O2}(3R_S) \times \exp(-R_p/R_{eff})$ with $N_{O2}(3R_S) = 3.0 \times 10^{10}$ molecules/cm^2 and $R_{eff} = 1.62R_S$. The total population of the scattered O_2 is about 17% of the main ring atmosphere. This component is primarily lost by re-impact with the ring particles but may be a dominant source of the O_2^+ ions detected outside of the rings by the CAPS instrument (Young et al., 2005; Tokar et al., 2005; Martens et al., 2008) and MIMI instrument (Krimigis et al., 2005).

Fig. 4a shows the two-dimensional cross-section of the azimuthally symmetric spatial distribution of the O_2^+ ions produced by photoionization and scattering by O_2. It is important to note that because of the vertical shift of the dipole moment, the ring plane is below the magnetic mid-plane by $0.04R_S$. As a result, new ions created in the thin disk of neutral O_2 on both sides of the ring plane will lead to a vertically asymmetric pattern of magnetic field-aligned motion. In the absence of gravity those created on the shadow side (or upper side) can oscillate about the magnetic equator and accumulate until they are scattered, but, as shown in Fig. 2 the addition of Saturn's gravity skews the ion motion so that impacts with the ring particles are important. In addition, since photo-ionization is the dominant ion formation process in our simulations, the ion formation rate on the shadow side is much less than that on the illuminated side except in the Cassini division. For these reasons fewer ions are found above the ring plane.

The motion of the pickup ions is controlled by the gravitational force and the electromagnetic (Lorentz) force. Therefore, it is seen that the inner region is roughly divided along the field line near $R_C \sim 1.7R_S$. Molecular oxygen ions created close to the gravitational equator and inside this radial distance primarily fall into the upper atmosphere of Saturn as indicated in Fig. 2. On the other hand, those created outside R_C have a probability of being absorbed by the ring particles except in those divisions in the ring in which the ring particle density is very small as in the Cassini Division at $2.0R_S$. Because of the small material content in the Cassini Division, the O_2^+ ion density reaches the maximum value of 250 cm^{-3}. It is also seen in Fig. 4a that there is a thin plasma disk just above the A ring plane with a vertical thickness of about $0.08R_S$ consistent with a small gravitational effect so that ions formed above the ring plane oscillate about the magnetic equator.

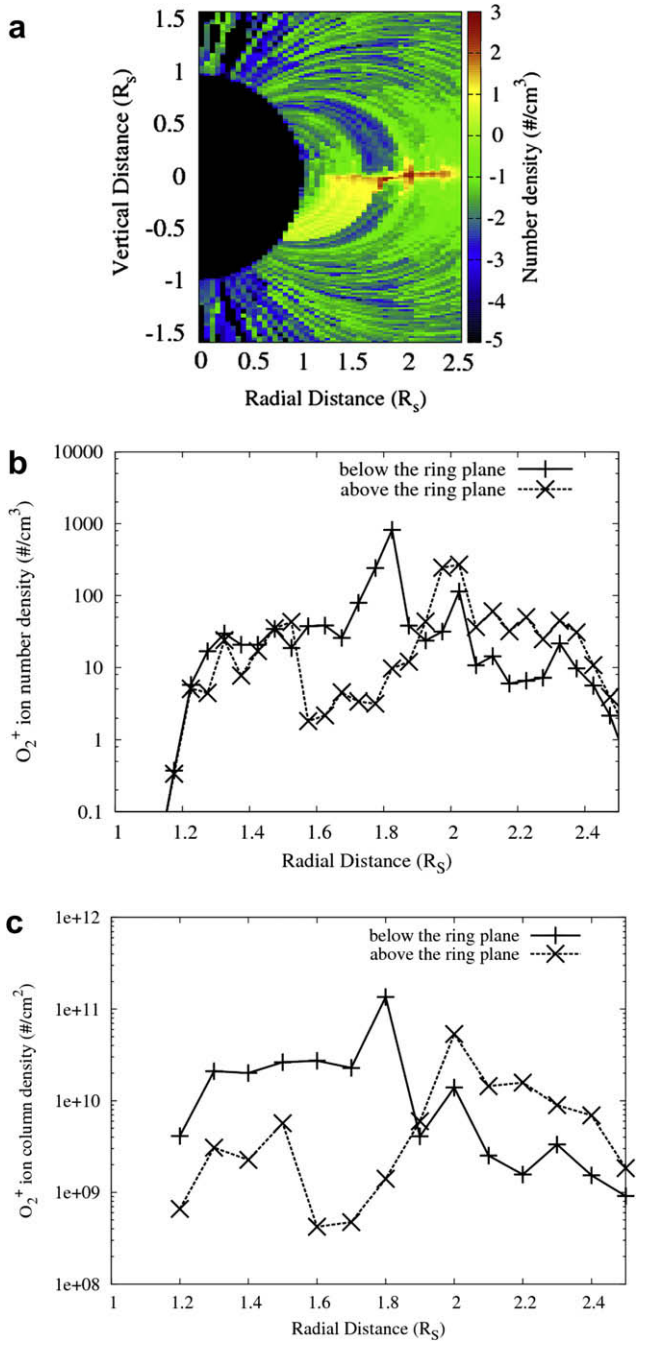

Fig. 4. (a) The O_2^+ ion number density in Log10 scale. (b) The O_2^+ ion number density at $0.01R_S$ below the ring plane and at $0.01R_S$ above the ring plane. (c) The O_2^+ ion column density above the ring plane and below the ring plane.

The O_2^+ ion number density and column density above and below the ring plane are shown in Figs. 4b and c, respectively. There is a much bigger difference above and below the ring plane in the B-ring region shown in both figures. This difference results from much less photoproduction of ions above the ring because of the large B-ring optical thickness. The large ion density in the Cassini Division is seen as is a density peak appears at $\sim 1.8R_S$. The ions created below the ring plane between ~ 1.7 and $1.8R_S$ can survive ring absorption because their oscillating centers are below the ring plane due to Saturn's gravity. In the A-ring region, the ion density above the ring plane is larger than below since ions created below the ring plane are subject to ring absorption when they move upward along the field lines.

Photoionization of the scattered neutral O_2 outside the main ring system produces a diffuse component of O_2^+ ions moving to higher altitudes. On the average, the lifetime of O_2 against photodissociation (time scale $\sim$162 days) and charge exchange collisional scattering (the average time scale $\sim$155 days near the ring plane) is about 79 days. Besides being scattered to escaping trajectories or large orbits outside the ring system, most of the scattered O_2 will re-impact the rings and recycled to the thermal population. In addition, a small fraction of the O_2 will be scattered into the Saturn's atmosphere. For the SOI condition, for a production rate of 9.7×10^{25} O_2 s^{-1}, the atmospheric injection rate of O_2 is about 1.4×10^{25} molecules s^{-1} while the magnetospheric injection rate is about 2.4×10^{25} molecules s^{-1}. Heating and acceleration of these ions will contribute to the energetic O_2^+ ions in the magnetosphere.

4. Seasonal variations

As Saturn orbits the sun, the solar incidence angle on the rings will change from illumination below the ring plane at a maximum angle of 25° to illumination above the ring plane at the same max-

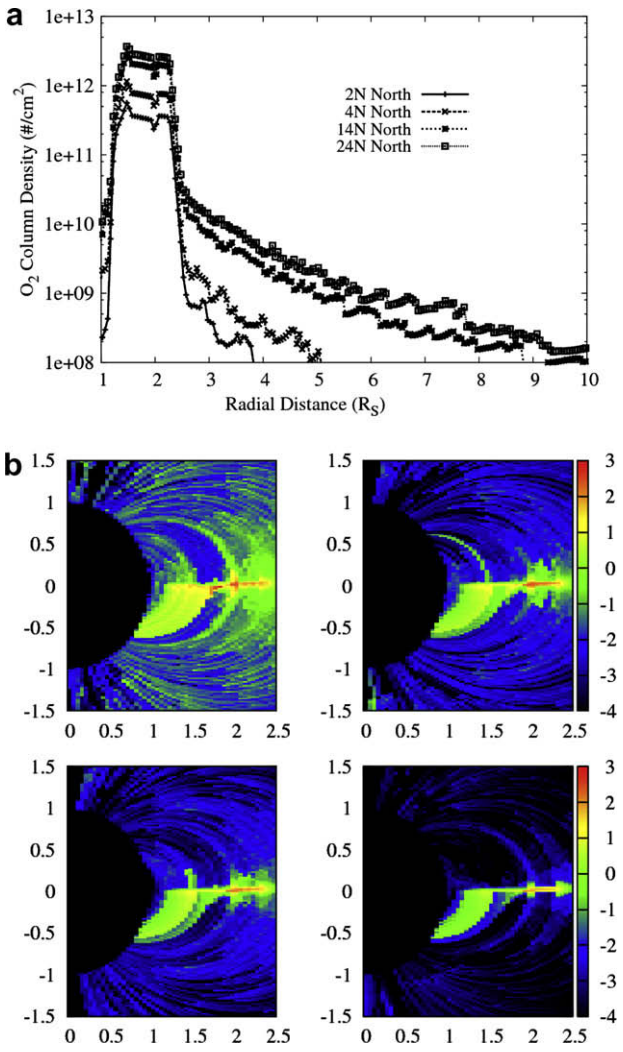

Fig. 5. (a) The neutral O_2 column density (molecules/cm^2) in four situations. (b) From top to bottom, the O_2^+ ion density for the solar incident angle $\sim$24° south of the ring plane (top-left), $\sim$24° north of the ring plane (top-right), $\sim$14° north of the ring plane (bottom-left), $\sim$4° north of the ring plane (bottom-right). The color is the number density (#/cm^3) in Log10 scale.

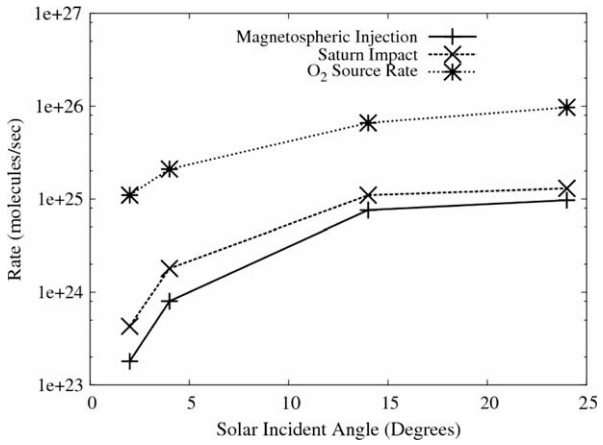

Fig. 6. The Saturn impact injection rates and the magnetospheric injection rates with variations of solar incident angles.

imum angle. Near equinox the incidence angle will become small, so that the ring atmosphere and ionosphere can change dramatically change as a function of the solar incidence angle.

The radial variation of the corresponding neutral O_2 column density is shown in Fig. 5a. Because of dependence of the solar flux on the insolation angle, the O_2 product ion rate from photosputtering should be proportional to $\cos\gamma$. Therefore, our simulations give ring ionospheric column densities that becomes smaller and smaller as Saturn approaches equinox. Fig. 5b shows the 2D spatial distribution of the O_2^+ ions when the solar incidence angle is 24° below the ring plane and 24°, 14° and 4° above the ring plane. It is interesting to note the ion density enhancement along the magnetic field line connected to the boundary between the B and C rings. This occurs because that the ions formed above the ring plane initially move downward and are absorbed by ring particles. As a consequence, the collisional scattering effect between the neutral O_2 and O_2^+ will also decrease in importance, producing a somewhat less (by a factor or about 2) magnetospheric injection and atmospheric precipitation. Fig. 6 shows the injection rates of Saturn impact and magnetospheric injections with variations of the solar incident angles. Both injections rates decrease with decreasing value of the solar incident angles.

5. Discussions

Johnson et al. (2006) proposed that the molecular oxygen atmosphere is primarily produced by the solar UV flux because the energetic particle flux over the main ring is small. In this situation, we show that the ion and neutral densities go through a minimum when Saturn's ring is edge-on. Because the scattering of O_2 into the magentopshere is a supply of O_2^+, such a variation in this heavy magentospheric molecular ion should be detectable by the CAPS and MIMI instruments. If this is found not to be the case, then either the ring atmosphere is not a dominant source of magnetospheric O_2^+ or another source mechanism for the ring atmosphere must be important. One such model is the formation of O_2 by chemical reactions on the surfaces of ring particles of the photodissociation products for the transient water vapor produced by meteorid impact (Ip, 1995). If the meteorite bombardment is a dominated mechanism, the neutral source rate will not vary with the solar insolation cycle. Ring surface chemistry is also important in determining the fate of the O, O^+ and O_2^+ that re-impact the ring particles and are absorbed. They can be recycled to O_2 by chemical reactions on the surface of ring particles (Ip, 1995). Johnson et al. (2006) also suggested that recycling of oxygen on the grains was important. However, the chemical state of these surfaces will also depend on the fate of the hydrogen atoms and molecules ejected (Johnson et al., 2006). This aspect will be considered in a subsequent paper.

In our present modeling, we ignore the electrostatic charge state of the icy grains. Since the ring particle surface are likely to be charged the emission of the photoelectrons, not considered here, planetary ionospheric plasma, and impact plasma generated by meteoroid impact are likely affected (Ip, 1984b). Charging would also affect the ion motion and the electrodynamic coupling of the rings with the planetary ionosphere (e.g., Graps et al., 2008; Goldreich and Farmer, 2007). For example, when the ions leave the ring plane in positive charging potential, the acceleration effect should be considered. Such effects affect the estimate of their atmospheric precipitation rate. Since only photoionization was included, the plasma-neutral atmosphere interactions outside of the ring plane were not considered in our modeling. Although the O_2 density distribution over the rings will only be marginally affected, the O_2^+ source rate in the magnetosphere depends directly on this interaction as electron impact and charge exchange are the dominant ionization mechanisms beyond 2.3 RS.

Cassini observations show that the brightness changes across the ring increase with the radial distance to a maximum at the outer edge of the A-ring (Esposito, 2005). It has been suggested that the outer edge could have more icy material. Jurac and Richardson (2007) proposed that the outer rings may show a brightening due to Enceladus-originating water deposition (see also Farrell et al., 2008).

Smith et al. (2007) have mentioned that models of solar heating of Saturn's upper atmosphere could not explain the high temperature (~400 K) observed independently in the polar regions and at 30° latitude. They speculated that an important candidate for the heat source is the magnetosphere, which injects energy into Saturn's upper atmosphere. Our work and the result of Luhmann et al. (2006) both showed that ions originated from the main rings mostly precipitated into Saturn's upper atmosphere at around 30° latitude, though with an enhancement in the southern hemisphere. It would be interesting to further study the relations between the temperatures in Saturn's atmosphere and the ring ion precipitations. Furthermore, precipitation into Saturn's upper atmosphere of ring-originated O_2, O and O^+, O_2^+ could also change the photochemical products. ISO observations (Feuchtgruber et al., 1997; de Graauw et al., 1997) have revealed the presence of water in Saturn's atmosphere. But these water molecules cannot originate without an external source as oxygen containing molecules are confined to the deep troposphere.

Moses et al. (2000) investigated the effect of an influx of oxygen on atmospheric chemistry. Their thermospheric model required a globally averaged oxygen influx of (2–4) 10^6 O atoms $cm^{-2}\,s^{-1}$. Using the nominal photo-decomposition source rate of $\sim 10^6 O_2/cm^2/s$ our simulations give a net oxygen influx in the form of O_2 that is about one order of magnitude smaller. However, as described earlier, the fate of the atomic oxygen absorb onto the ring particle surfaces was not considered in these simulations, but can change the result significantly. For instance, in order to explain the Cassini ion density data, Johnson et al. (2006) required an O_2 source rate large than that estimated from by photodecomposition data. Assuming this was due to recycling of oxygen on the ring particle surfaces their enhancement factor was ~>10. Prior to Cassini data Ip (1995) estimated a recycling rate that would result in an enhancement factor ~5. Therefore, in the absence of other effects our densities should be scaled upward by a factor of ~5–10. If such increases are correct then the ring atmosphere source rate for oxygen precipitation into Saturn's atmosphere will approach that required by Moses et al. (2000). Simulations of the chemistry of the returning oxygen on the ring particle surfaces are in progress. Since these surface also contain contaminants which compete for

the oxygen (Cuzzi et al., 2009—chap in Cassini book), the best constraint is a detailed comparison of the ring atmosphere model to the CAPS ion density data. Of course, alternative oxygen source have been proposed such as the injection of charged small dust grains into Saturn's atmosphere could play a role in this context (Connerney and Waite, 1984).

6. Summary

In this paper we carried out new simulations of the neutral and ion components of Saturn's ring atmosphere with emphasis on molecular oxygen neutrals and ions. These simulations confirm basic picture developed by the earlier models but are carried out in greater detail. It is shown that:

1. The neutral O_2 atmosphere is similar above and below the ring plane but is strongly dependent on Saturn's orbital position. We show that the neutral O_2 density goes through a minimum when Saturn's rings are edge-on, if the radiolysis decomposition of ices by solar photons is the main source mechanism.
2. Inside of $\sim 1.7R_S$, there is a very dramatic asymmetry of the ring ionosphere between the northern and southern hemispheres, with a much larger southern hemisphere density. The ion scale height increases with increasing radial distances outside of $\sim 1.7R_S$.
3. The neutral O_2, that are scattered into the outer magnetosphere, can be ionized by photons and magnetospheric electrons and ions and, therefore, are a source of magnetospheric O_2^+ detected by Cassini CAPS and MIMI. We also have shown that measured variations in the net magnetospheric O_2^+ content over Saturn's seasons can help determine whether the proposed model is valid.
4. The ring atmosphere is also a source of neutral oxygen for Saturn's atmosphere. In the absence of recycling of oxygen on the surfaces of the ring particles, we obtain a minimum source strength of 2.8×10^{25} O s^{-1} at maximum illumination. Therefore, either recycling is important or another source of oxygen is required to explain the presence of oxygen containing molecules in Saturn's thermosphere.

References

Bouhram, M., Johnson, R.E., Berthelier, J.-J., Illiano, J.-M., Tokar, R.L., Young, D.T., Crary, F.J., 2006. A test-particle model of the atmosphere/ionosphere system of Saturn's main rings. Geophys. Res. Lett. 33, L05016.

Carlson, R.W., 1980. Photosputtering of Saturn's rings. Nature 283, 461–463.

Coates, A.J., McAndrews, H.J., Rymer, A.M., Young, D.T., Crary, F.J., Maurice, S., Johnson, R.E., 2005. Plasma electrons above Saturn's main rings: CAPS observations. Geophys. Res. Lett. 32, L14S09.

Connerney, J.E.P., Waite, J.H., 1983. New model of Saturn's ionosphere with an influx of water from the rings. Nature 312, 136–138.

Connerney, J.E.P., Acuna, M.H., Ness, F.N., 1983. Currents in Saturn's magnetosphere. J. Geophys. Res. 88, 8779–8789.

Cuzzi, J., Dones, L., Clark, R., Johnson, R., Spilker, L., French, R., Marouf, E., Filacchione, G., 2009. Ring Particle Composition and Size Distribution. Saturn after Cassini-Huygens, In press.

de Graauw, T., and 18 colleagues, 1997. First results of ISO-SWS observations of Saturn: Detection of CO_2, CH_3C_2H, C_4H_2 and tropospheric H_2O. A&A 321, L13–L16.

Esposito, L.W., Ocallaghan, M., Simmons, K.E., Hord, C.W., West, R.A., Lane, A.L., Pomphrey, R.B., Coffeen, D.L., Sato, M., 1983. Voyager photopolarimeter stellar occultation of Saturn's rings. J. Geophys. Res. 88, 8643–8649.

Esposito, L.W., and 15 colleagues, 2005. Ultraviolet imaging spectroscopy shows an active saturnian system. Science 307, 1251–1255.

Farrell, W.M., Kaiser, M.L., Gurnett, D.A., Kurth, W.S., Persoon, A.M., Wahlund, J.E., Canu, P., 2008. Mass unloading along the inner edge of the Enceladus plasma torus. Geophys. Res. Lett. 35, L02203.

Feuchtgruber, H., Lellouch, E., de Graauw, T., Bezard, B., Encrenaz, T., Griffin, M., 1997. External supply of oxygen to the atmospheres of giant planets. Nature 389, 159–162.

Goldreich, P., Farmer, A.J., 2007. Spontaneous axisymmetry breaking of the external magnetic field at Saturn. J. Geophys, Res. 112, A05225.

Graps, A.L., Jones, G.H., Juhasz, A., Horanyi, M., Havnes, O., 2008. The charging of planetary rings. Space Sci. Rev. 137, 435–453.

Huebner, W.F., Keady, J.J., Lyon, S.P., 1992. Solar photo rates for planetary atmospheres and atmospheric pollutants. Ap&SS 195, 1–295.

Ip, W.-H., 1983. Collisional interactions of ring particles – The ballistic transport process. Icarus 54, 253–262.

Ip, W.-H., 1984a. Plasmatization and recondensation of the saturnian rings. Nature 320, 143–145.

Ip, W.-H., 1984b. Electrostatic charging of the rings of Saturn: A parameter study. J. Geophys. Res. 89, 3829–3836.

Ip, W.-H., 1984c. On the equatorial confinement of thermal plasma generated in vicinity of the rings of Saturn. J. Geophys. Res. 89, 395–398.

Ip, W.-H., 1995. Exospheric systems of Saturn's rings. Icarus 115, 295–303.

Ip, W.-H., 2005. An update on the ring exosphere and plasma disc of Saturn. Geophys. Res. Lett. 32, L13204.

Johnson, R.E., Quickenden, T.I., 1997. Photolysis and radiolysis of water ice on outer solar system bodies. J. Geophys. Res. 102, 10985–10996.

Johnson, R.E., Boring, J.W., Reimann, C.T., Barton, L.A., Sieveka, J.W., Garrett, J.W., Farmer, K.R., Brown, W.L., Lanzerotti, L.J., 1983. Plasma ion-induced molecular ejection on the Galilean satellites – Energies of ejected molecules. Geophys. Res. Lett. 10, 892–895.

Johnson, R.E., Liu, M., Sittler, E.C., 2005. Plasma-induced clearing and redistribution of material embedded in planetary magnetospheres. Geophys. Res. Lett. 32, L24201.

Johnson, R.E., Luhmann, J.G., Tokar, R.L., Bouhram, M., Berthelier, J.J., Sittler, E.C., Cooper, J.F., Hill, T.W., Crary, F.J., Young, D.T., 2006. Production, ionization and redistribution of Saturn's O2 ring atmosphere. Icarus 180, 393–402.

Krimigis, S.M., and 31 colleagues, 2005. Dynamics of Saturn's magnetosphere from MIMI during Cassini's orbital insertion. Science 307, 1270–1273.

Luhmann, J.G., Johnson, R.E., Tokar, R.L., Ledvina, S.A., Cravens, T.E., 2006. A model of the ionosphere of Saturn's rings and its implications. Icarus 181, 465–474.

Martens, H.R., Reisenfeld, D.B., Williams, J.D., Johnson, R.E., Smith, H.T., 2008. Observations of molecular oxygen ions in Saturn's inner magnetosphere. Geophys. Res. Lett. 35, L20103.

Morfill, G.E., Fechtig, H., Grun, E., Goertz, C.K., 1983. Some consequences of meteoroid impacts on Saturn's rings. Icarus 55, 439–447.

Moses, J.I., Lellouch, E., Bezard, B., Gladstone, G.R., Feuchtgruber, H., Allen, M., 2000. Photochemistry of Saturn's atmosphere: II. Effects of an influx of external oxygen. Icarus 45, 166–202.

Smith, C.G.A., Aylward, A.D., Millward, G.H., Miller, S., Moore, L.E., 2007. An unexpected cooling effect in Saturn's upper atmosphere. Nature 445, 399–401.

Tokar, R.L., and 12 colleagues, 2005. Cassini observations of the thermal plasma in the vicinity of Saturn's main ring and the F and G rings. Geophys. Res. Lett. 32, L14S04.

Waite Jr., J.H., and 10 colleagues, 2005. Oxygen ions observed near Saturn's A ring. Science 307, 1260–1262.

Westley, M., Baragiola, R.A., Johnson, R.E., Baratta, G., 1995. Photo desorption from low temperature water ice: Astrophysical implications. Nature 373, 405–407.

Young, D.T., and 42 colleagues, 2005. Composition and dynamics of plasma in Saturn's magnetosphere. Science 307, 1262–1266.